



Experimental and mechanism study of C_f/SiC undergoing longitudinal-torsional ultrasonic vibration-assisted grinding

Xiaobo Wang¹ · Mingqiang Wu¹ · Chaosheng Song¹ · Bo Zhao¹

Received: 21 April 2023 / Accepted: 17 July 2023 / Published online: 24 July 2023
© The Author(s), under exclusive licence to Springer-Verlag London Ltd., part of Springer Nature 2023

Abstract

Ceramic matrix composites (CMCs) with carbon fiber reinforcement are widely used in the aircraft industry and other important defense industries due to their superior performance. To investigate the factors affecting the grinding force and surface quality of 2.5D needled C_f/SiC material, the motion equation of abrasive particles under longitudinal-torsional ultrasonic vibration was established using kinematic analysis, and the trajectory analysis of abrasive particles was carried out using MATLAB simulation. The grinding force, surface topography, and roughness of conventional grinding (CG) and longitudinal-torsional ultrasonic vibration-assisted grinding (L-TUVAG) were analyzed and evaluated to explore the process mechanism of C_f/SiC material damage. An improved processing technique and parameters for processing were proposed. The findings show that the principal pathways for material removal during grinding are matrix breaks, interfacial debonding, fiber damage, and fractures. Grinding parameters have a significant influence on the quality of the processing surface. The surface topography steadily improves during the grinding process as the grinding wheel speed increases. However, the feed speed and grinding depth have a reverse impact. High-speed micro-grinding can significantly improve grinding efficiency and surface processing quality. L-TUVAG has a lower grinding force than CG by a factor of 16.16% to 35.82%, and the surface processing quality is correspondingly better. These discoveries enable the prediction of surface morphology and roughness characteristics of materials. And provide important technological support for improving the processing quality of CMCs.

Keywords Kinematic analysis · Grinding force · Longitudinal-torsional ultrasonic vibration · Surface topography · Roughness

1 Introduction

Fiber-reinforced CMCs are a new type of low-density thermal structural material that has developed rapidly in recent years [1–3]. In order to create this high-performance composite material, carbon fiber strands are implanted into the SiC matrix after being textured to fit a specific structure [4, 5]. It combines the SiC matrix's excellent chemical and thermal stability with carbon fiber's superior mechanical properties. Its benefits include high-temperature resistance, low density, high strength, resistance to chemical corrosion, resistance to wear, and the lack of deterioration of any of these features over time [6–9]. Additionally, due to the fiber's toughening effect, CMCs' fracture toughness has been significantly

increased, opening up a variety of application possibilities in fields such as nuclear energy, high-end automobile brake systems, aircraft thermal protection systems, gas turbine turbines, and engine combustion chambers [10, 11].

For C_f/SiC materials, there is a relatively weak bond between the matrix and the fiber. There is only one strengthening direction in unidirectional C_f/SiC materials [12]. The range of uses for composite materials is constrained by this flaw. Although the performance of 2D C_f/SiC has been enhanced in two directions, their strength and wear resistance still fall short of the requirements. In addition, 3D C_f/SiC are expensive, and their range of use is constrained. 2.5D C_f/SiC materials are proposed to lower costs while maintaining material strength and usage requirements [13–15]. Also included in this laminated composite construction are short fiber needles. Because of the way the suture is built, bending the fibers considerably boosts the composite's toughness. Consequently, in this research, the 2.5D needled C_f/SiC materials were examined [16].

✉ Mingqiang Wu
wmq@home.hpu.edu.cn

¹ School of Mechanical and Power Engineering, Henan Polytechnic University, Jiaozuo 454003, Henan, China

The majority of CMCs are created by near-net molding; nevertheless, high dimensional accuracy and surface quality criteria must be reached by secondary processing in order to meet the demands of high-precision assembly and usage [17]. Due to the high hardness, multi-phase structure, and anisotropy of this type of material, many defects are easily formed on the surface during traditional processing, such as severe tool wear, low processing efficiency, surface cracks, broken, chipping, and other defects [18].

L-TUVAG is a leading-edge processing technique for difficult-to-cut materials that performs very well in terms of lowering cutting force and temperature, decreasing tool wear and extending tool life, enhancing the machinability of the material, and enhancing machining surface quality [19–21]. It is commonly employed in the creation of glass, ceramic, ceramic matrix composites, metal matrix composites, titanium, nickel-based superalloys, and carbon fiber-reinforced polymers [22–24].

Choudhary et al. [25] performed a high-speed grinding experiment on C_f/SiC materials and discovered that the considerable thickness of undeformed chips rises the formation of surface defects. Azarhoushang [26] investigated how ultrasonic vibration affected surface roughness of C_f/SiC materials by using a self-developed ultrasonic device to actualize the workpiece material's ultrasonic vibration. According to this research, ultrasound vibratory can reduce surface roughness by approximately 30% and grinding force by around 20%. Bertsche et al. [27] performed various combinations of traditional grinding and ultrasonic-assisted grinding tests on CMCs and studied grinding force, tool wear, and surface roughness. The following findings have been reached: Ultrasonic-assisted grinding lowered grinding forces by 20% and 9% in the F_y and F_z directions, in addition to reduced tool wear by 36%. Yuan et al. [28] investigated ultrasonic milling. They developed the dynamic cutting force model for side milling and tested its veracity. When the experimental and simulated cutting force data are compared,

the errors for most parameter groups are found to be less than 10%. Liu et al. [29] investigated the material removal form and fracture behavior of 2D C_f/SiC materials. Brittle fracture is the main type of removal, and the main removal methods are interface debonding, fiber fracture, and matrix cracking. Qu et al. [30] ground unidirectional C_f/SiC ceramic matrix composites and discovered that when cracks propagate to carbon fibers, they alter, and the grinding debris comprises silicon carbide matrix fragments and carbon fiber fragments. Distinct fiber angles have distinct material removal shapes.

To determine the effect of grinding parameters (feed speed, grinding wheel speed, and grinding depth) on grinding force, surface topography, and three-dimensional surface roughness, 2.5D needled C_f/SiC composites conducted L-TUVAG and CG experiments. The influence of ultrasonic vibration on material removal is explored, and the removal process of material is revealed under ultrasonic vibration. Provide a more efficient technique of production and processing.

2 L-TUVAG theoretical model

2.1 L-TUVAG abrasive particles motion trajectory

On the basis of CG, ultrasonic vibration will alter the abrasive particles' motion paths and the distance at which they make contact with the materials, which will then have an impact on the grinding law. This paper mainly studies the processing of materials by L-TUVAG. The grinding wheel rotates while being accompanied by longitudinal ultrasonic vibration along the axial direction, torsional ultrasonic vibration around the z -axis, and maintaining horizontal feed movement along the workpiece. The abrasive particles trajectory in L-TUVAG, therefore, combines four different types of motion. In Fig. 1a, V_c is the spindle speed; V_w is the feed speed; a_p is the grinding depth; A_1 is the torsional

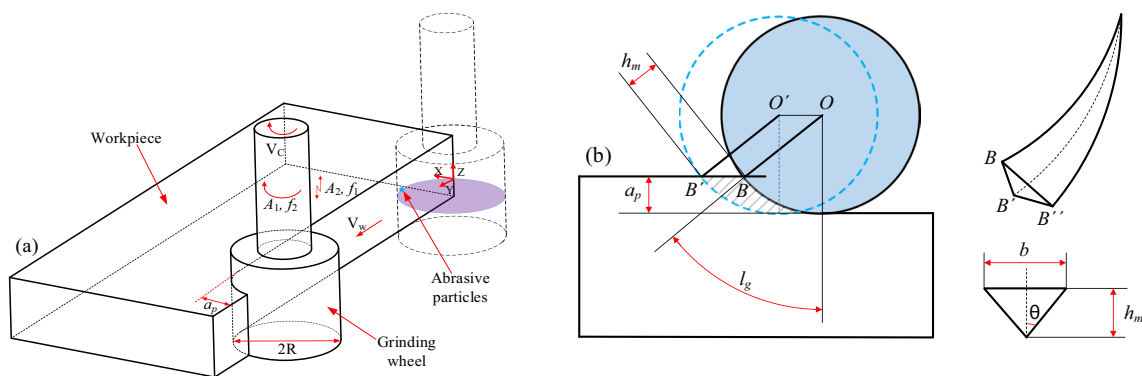


Fig. 1 L-TUVAG processing. **(a)** Schematic diagram. **(b)** Undeformed chip thickness

ultrasonic vibration; A_2 is the longitudinal ultrasonic vibration; f is the ultrasonic vibration frequency; and R is the grinding wheel radius.

The point O of the workpiece and the abrasive particle in the same plane are taken as the origin, the V_w direction as the Y axis, the perpendicular to the V_w direction as the X axis, and the grinding wheel axis direction as the Z axis. The equation of motion of the abrasive particles around the grinding wheel axis is as follows:

$$\begin{cases} x(t) = R(1 - \sin(2\pi V_c t)) \\ y(t) = R\cos(2\pi V_c t) + V_w t \end{cases} \quad (1)$$

After including longitudinal-torsional ultrasonic vibration:

$$\begin{cases} x(t) = R\cos[\omega t + A_1 \sin(2\pi f_1 t + \varphi)]/R \\ y(t) = R\sin[\omega t + A_1 \sin(2\pi f_1 t + \varphi)]/R + V_w t \\ z(t) = A_2 \sin(2\pi f_2 t) \end{cases} \quad (2)$$

Using the parameters in Table 1, the simulation results are shown in Fig. 2. The kinematics simulation is carried out using MATLAB. When the parameters are the same, L-TUVAG has a longer trajectory of abrasive particles than CG. Therefore, L-TUVAG can increase the grinding time of the abrasive, reduce the residual height of the material on the workpiece surface, and then improve the surface quality. While simultaneously producing periodic contact-separation motion under longitudinal-torsional ultrasonic vibration, the workpiece, and abrasive particles can reduce friction between the workpiece surface and the abrasive cutting edge. Surface roughness and grinding force are both reduced.

3 L-TUVAG abrasive grinding arc length

Velocity equation of abrasive particles under longitudinal-torsional ultrasonic vibration:

$$\begin{cases} V_x = [R\omega + 2A_1\pi f_1 \cos(2\pi f_1 t + \varphi)] \sin[\omega t + A_1 \sin(2\pi f_1 t + \varphi)]/R \\ V_y = [R\omega + 2A_1\pi f_1 \cos(2\pi f_1 t + \varphi)] \cos[\omega t + A_1 \sin(2\pi f_1 t + \varphi)]/R + V_w \\ V_z = 2A_2\pi f_2 \sin(2\pi f_2 t) \end{cases} \quad (3)$$

The grinding linear velocity V_s of abrasive particles includes linear velocity V_g of grinding wheel rotation and linear velocity V_t of ultrasonic vibration:

$$V_s = V_g + V_t = R\omega + 2\pi f_1 A_1 \cos(2\pi f_1 t) \quad (4)$$

Grinding arc length of abrasive particles under longitudinal-torsional ultrasonic vibration:

$$S_t = \int_0^t \sqrt{V_w^2 + V_s^2 + 2V_w V_s \cos[\omega t + A_1 \sin(2\pi f_1 t + \varphi)]/R + (2\pi f_2 A_2)^2 \cos^2(2\pi f_2 t)} dt \quad (5)$$

Grinding arc length of abrasive particles under CG ($A_1 = A_2 = 0$):

$$S_t = \int_0^t \sqrt{V_w^2 + V_g^2 + 2V_w V_g \cos(\omega t)} dt \quad (6)$$

The longitudinal-torsional ultrasonic horn with single excitation is used in the experiment.

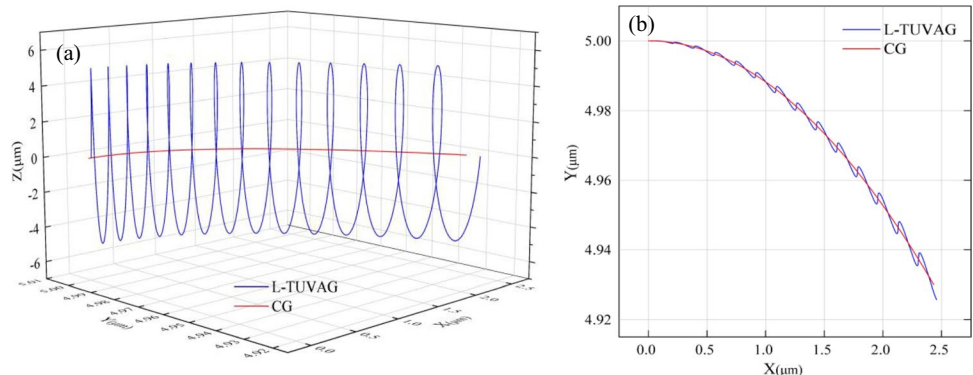
$$f_1 = f_2 = f \quad (7)$$

The cutting arc length per unit time of L-TUVAG is related to grinding parameters. It also has a great relationship with the frequency and amplitude. With the increase in amplitude and frequency, the cutting arc length of abrasive particles becomes longer.

Table 1 Simulation parameters of abrasive particle motion trajectory

Radius of grinding wheel (mm)	Grinding wheel speed (rpm)	Feed speed (mm/min)	Ultrasonic frequency (kHz)	Longitudinal amplitude (μm)	Torsional amplitude (μm)	Phase difference
8	4000	150	31	4	3	Pi/2

Fig. 2 (a) 3D abrasive particle motion trajectory (b) X-Y plane motion trajectory



4 L-TUVAG maximum undeformed cutting thickness

Figure 1b depicts the shape of the maximum undeformed chip piece, which is approximately a triangular pyramid. On the basis of routine grinding, the L-TUVAG abrasive's real grinding width is increased by $A_1 \sin(\omega t)$, and the average effective grinding width of the abrasive is achieved.

$$b_m = 2h_m \tan\theta + A_1/\sqrt{2} \quad (8)$$

According to the research of Malkin et al. [31], the maximum undeformed cutting thickness h_m can be expressed as:

$$h_m = \frac{2}{C} \frac{V_w}{b_m V_c} \left(\frac{a_p}{d_e} \right)^{1/2} \quad (9)$$

$$C = \frac{2}{d_f (4\pi/3\lambda)^{2/3}} \quad (10)$$

d_e is the equivalent diameter of the grinding wheel; d_f is the equivalent diameter of the abrasive grain; and λ is the volume fraction. In L-TUVAG, h_m is connected to the axial amplitude A_1 , the grinding parameters, and the equivalent grinding wheel diameter d_e . H_m decreased when V_c and A_1 grew, while it increased as V_w and a_p increased. The increase in h_m will increase the normal force, and the larger normal force will produce long cracks, resulting in more defects and poorer surface quality on the machined surface.

5 Experiment material and methods

5.1 Research material

In the experimental material, the acupuncture fiber runs through the whole fiber and matrix layer. It is created using a combination of the PIP and CVI methods [2, 5]. According

to Fig. 3, the substance is made of reinforcement of carbon fibers composed of needled fibers, 0° and 90° fiber layers, and the SiC matrix. Each layer contains a unidirectional distribution of $0^\circ/90^\circ$ fiber sections.

6 Grinding conditions

The size of the workpiece is 20 mm × 15 mm × 10 mm. The vibration system has a rated power of 300 W and a produced ultrasonic vibration frequency of 16–35 kHz. This experiment aims to investigate the connection between material surface quality and grinding parameters. The grinding is done in the orthogonal surface's direction, and as the grinding wheel turns, the fiber bundle experiences tensile and shear forces. Grinding is done with a diamond grinding wheel that has been electroplated, and the parameters are shown in Table 2. The grinding wheel is fixedly connected to the handle through a collet. The workpiece is fixed to the fixture, which is fixed to the Kistler9257B piezoelectric dynamometer, and this is fixed to the platform of the machine tool by nuts, it is chosen to use a dynamometer to measure the normal grinding force (F_n) and tangential grinding force (F_t). The L-TUVAG experimental platform and schematic diagram are shown in Fig. 4, field emission scanning electron microscope (Merlin Compact) and digital microscope (VHX-1000E) were used to examine the surface topography during this process. Using a measuring laser microscope, the OLS51003D, surface roughness was calculated. This 200 μm × 200 μm area is scanned. To reduce measurement errors, surface roughness parameters were measured three times. The average of the three measurements is then used to calculate the final result.

The simple surface roughness R_a can no longer be employed as an assessment criterion due to the anisotropic properties of C_f/SiC materials. The 3D surface roughness S_a is measured over the entire measurement zone to more

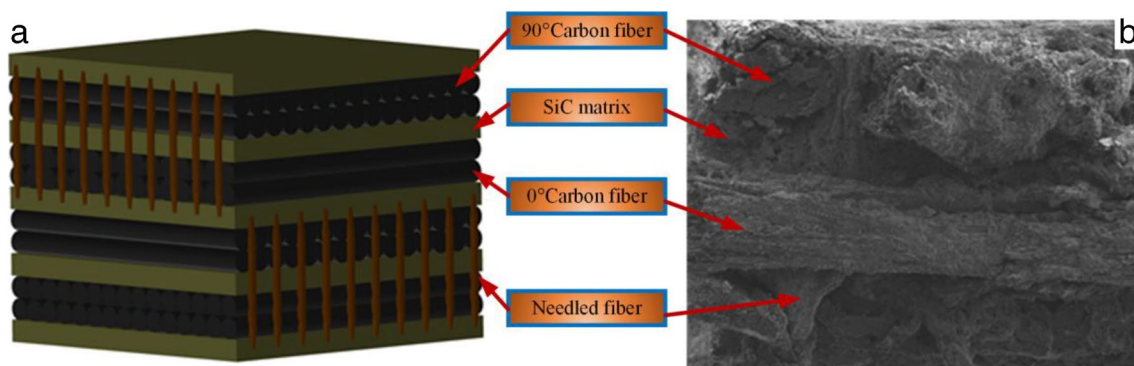


Fig. 3 Schematic diagram (a) and SEM image (b)

Table 2 Experimental conditions

Type	Parameters	Value
Grinding wheel	Diamond grinding wheel	
	Diameter (mm)	8
	Granularity (#)	200
Grinding parameters	V_c (rpm)	2000, 3000, 4000, 5000
	a_p (μm)	3, 6, 9, 12
	V_w (mm/min)	50, 100, 150, 200
	A_1 (μm)	0, 3
	A_2 (μm)	0, 4

properly depict the topography of the surface of the C_f/SiC material [10]. It is one of the most often used characteristics and represents the mean of the mean plane’s height difference. It produces consistent findings and is unaffected by measuring noise and scratches.

7 Results and analysis

7.1 Grinding force

As shown in Fig. 5a, the F_n and F_t of both CG and L-TUVAG exhibit a decreasing trend as the rotational speed of the grinding wheel rises, and under the same circumstances, the grinding force of L-TUVAG is lower than that of CG. The grinding force can be efficiently decreased by raising the spindle speed while all other factors remain constant. The reason is that as spindle rotation speed rises, the largest undeformed chip thickness diminishes and the contact arc length between abrasive particles and workpiece material grows longer per unit of time; The temperature at the region where the grinding wheel and workpiece’s material come into contact rises with increasing rotational speed, which lowers the coefficient of friction between abrasive particles and materials. Due to the combined effect of these two factors, surface roughness and grinding force both diminish as spindle rotational speed increases. In addition, when compared to CG, L-TUVAG can

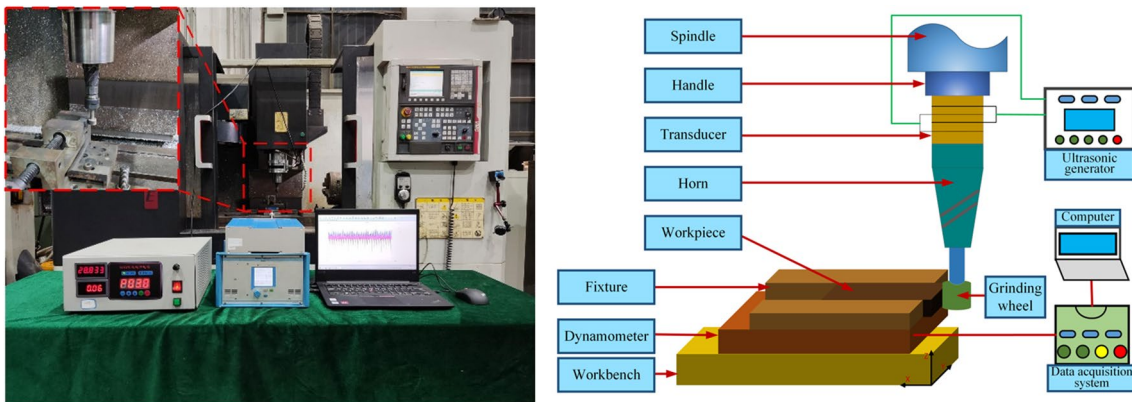
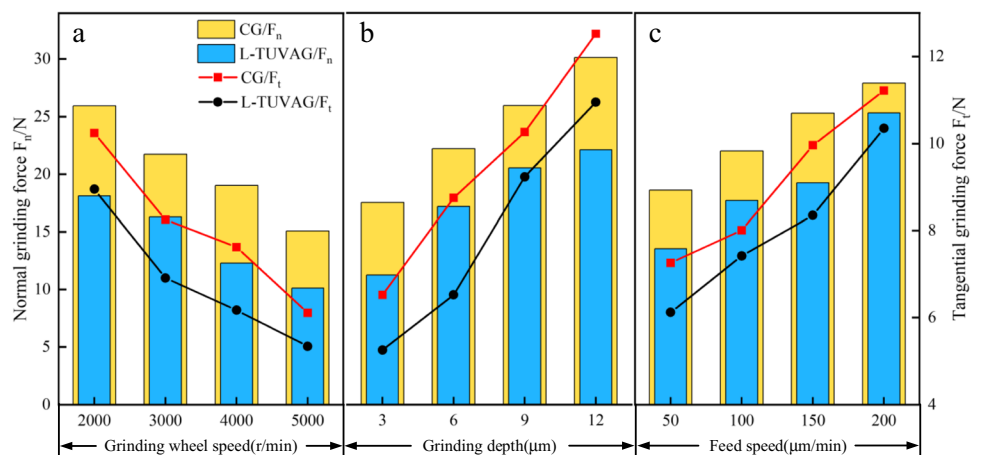


Fig. 4 Experimental site and schematic diagram

Fig. 5 Effect of grinding parameters: (a) $a_p = 6 \mu\text{m}$, $V_w = 100 \text{ mm/min}$; (b) $V_c = 3000 \text{ rpm}$, $V_w = 100 \text{ mm/min}$; (c) $V_c = 3000 \text{ rpm}$, $a_p = 6 \mu\text{m}$



lower F_n by up to 32.94% and F_t by up to 19.03%. This is because the use of high-frequency ultrasonic vibration alters the material removal mechanism, making it simpler for the workpiece to fracture and generate chips.

This is shown in Fig. 5b. As grinding depth becomes deeper, F_n and F_t in both CG and L-TUVAG increase. As the depth of the grind grows, the h_m and material removal rate increase, and the strain that needs to be overcome during material removal increases. And on the other side, the increase in grinding depth leads to faster tool wear and increased friction between tool chips, resulting in increased grinding force and poorer surface processing quality. As illustrated in Fig. 7, the surface is prone to flaws such as fiber extraction and edge collapse at this time. When compared to CG at the same grinding depth, L-TUVAG reduces both F_n and F_t , with a maximum reduction of 35.82% in F_n and a maximum reduction of 19.48% in F_t .

The variation curve of grinding force with feed speed is shown in Fig. 5c. The results reveal that when feeding speed increases, F_n and F_t rise. Increased feed speed leads to an increased material removal rate, which necessitates greater energy consumption during the grinding process. Furthermore, when the feed speed increases, so does tool wear and the rubbing of the tool against the chip, causing F_n and F_t to rise. Under the same processing circumstances as CG, L-TUVAG reduces both normal and tangential pressures, with a maximum reduction in F_n of 27.23% and a maximum reduction in F_t of 16.16%.

8 2D and 3D Surface topography

Brittle fracture is the main removal method for ceramics as a representative of brittle materials. Many grooves are evident on the ceramic surface following the material's grinding with a diamond grinding wheel. The addition of carbon fibers, however, greatly impacts the fracture mechanism of C_f/SiC material. Because of their differing characteristics, silicon carbide and carbon fiber have diverse and asynchronous removal patterns.

Figures 6 and 9 depict the 2D and 3D surface topography of CG and L-TUVAG at 2000 rpm and 5000 rpm grinding wheel speeds, respectively. The principal damage mechanisms, including matrix breaks, interfacial debonding, fiber damage and fractures, are depicted in the figure. When the grinding wheel speed is adjusted to 2000 rpm, several cracks can be seen. According to the 3D surface, the wave crests are rutted and uneven, and surface texture processing is poor. The area of fiber damage increases as the speed does as well. In contrast, the number of cracks dropped, the number of pits decreased, and the surface topography improved. This demonstrates that surface texture is improved by grinding at a higher speed. The grinding process accelerates and approaches the real particle size when the wheel speed is increased. This results in the material removal property turning plastic and the grinding groove becoming shallow and narrow, considerably enhancing the grinding quality.

In addition to the stepped fracture of fiber on the machined surface, as illustrated in Fig. 6c, there are grooves and broken carbon fibers left by lots of carbon fibers peeling

Fig. 6 2D surface topography; $a_p = 6 \mu\text{m}$, $V_w = 100 \text{ mm/min}$; (a) $V_c = 2000 \text{ rpm}$; (b) $V_c = 5000 \text{ rpm}$; (c) CG; (d) L-TUVAG

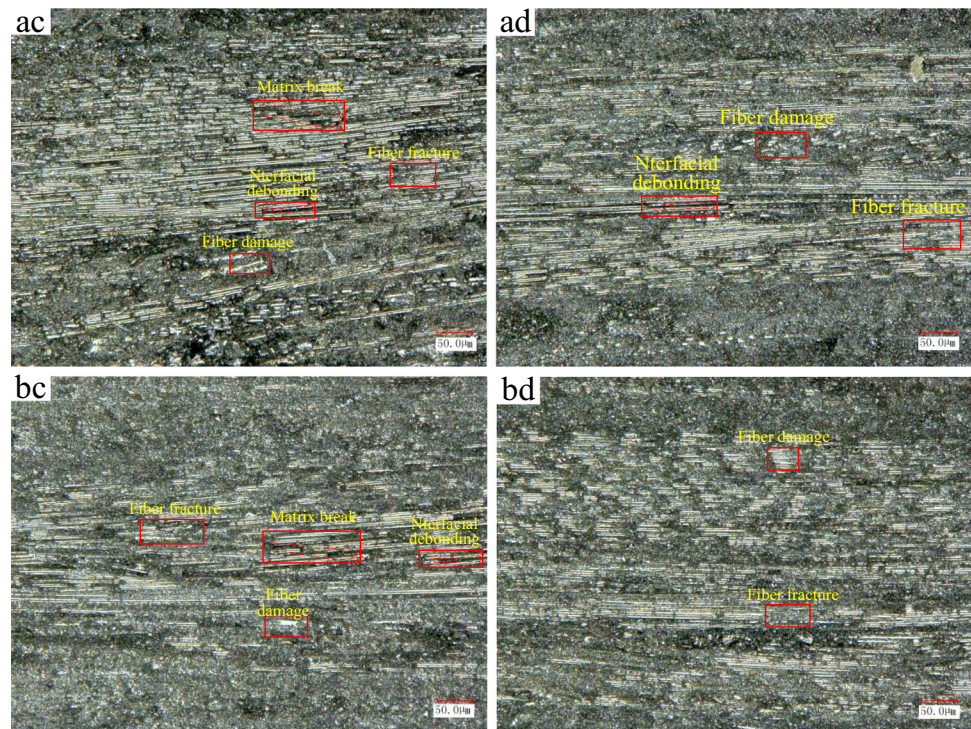
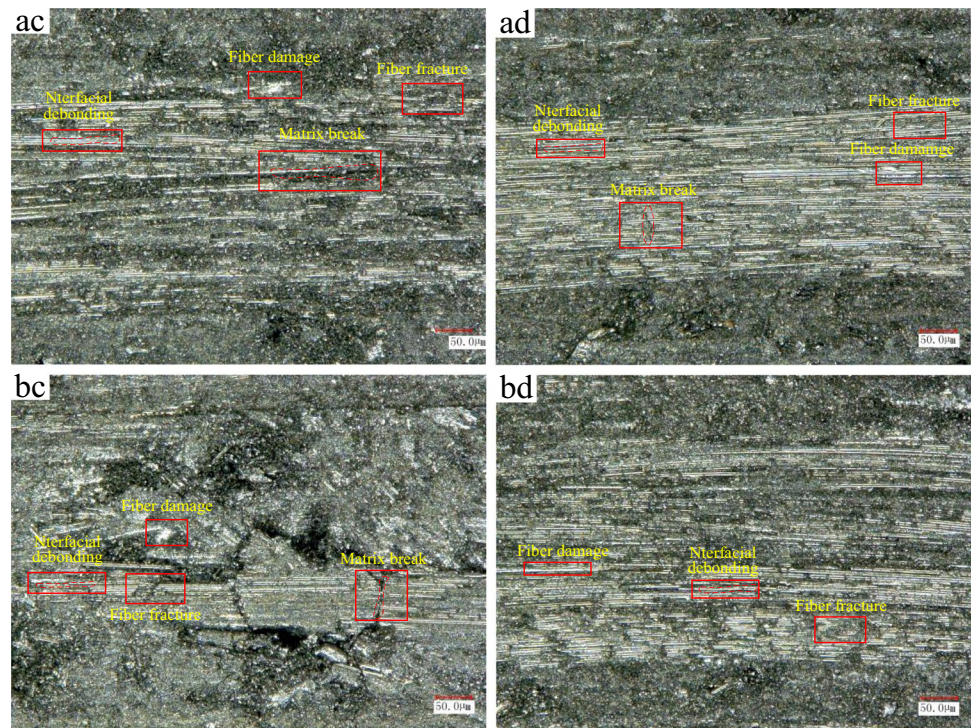


Fig. 7 2D surface topography; $V_c = 3000$ rpm, $V_w = 100$ mm/min; (a) $a_p = 3$ μm ; (b) $a_p = 12$ μm ; (c) CG; (d) L-TUVAG



off from the matrix; Fig. 6d shows that in L-TUVAG, the carbon fiber detached from the SiC matrix is completely removed, and the carbon fiber peeling is reduced, there are fewer spalled grooves in the SiC matrix, and the material's surface quality is improved. The maximum height of 3D surface topography for CG and L-TUVAG, respectively, reduces from 23.36 to 12.44 μm and 15.03 to 11.18 μm when this grinding wheel speed is 2000–5000 rpm.

Surface topography for CG and L-TUVAG at various depths of grinding is shown in Figs. 7 and 10. The fundamental grinding mechanisms remain matrix breaks, interfacial debonding, fiber damage and fractures. The main material removal mechanism does not alter as the profundity of the grinding increases. However, the distribution of the various types of damage does alter across the entire machined surface. For instance, the fiber's wear area gradually reduces while the rate of crack formation rises. As the depth of the grinding increases, the increased normal pressure causes cracks to spread. The fiber separates from the matrix under the influence of strong shear forces. Debonding interface is caused by shear force. The deterioration of the surface topography can be observed on the 3D surface. There are a lot of fiber fracture areas that are simple to discover when the grinding depth is 12 μm .

Figure 7d illustrates the carbon fiber's short fracture shape. Additionally, when the same grinding conditions are used, L-TUVAG results in fewer and more minor cracks. This is because the intermittent high-frequency impact from L-TUVAG on a material's surface can decrease the effects of material anisotropy on grinding. By being chopped off into

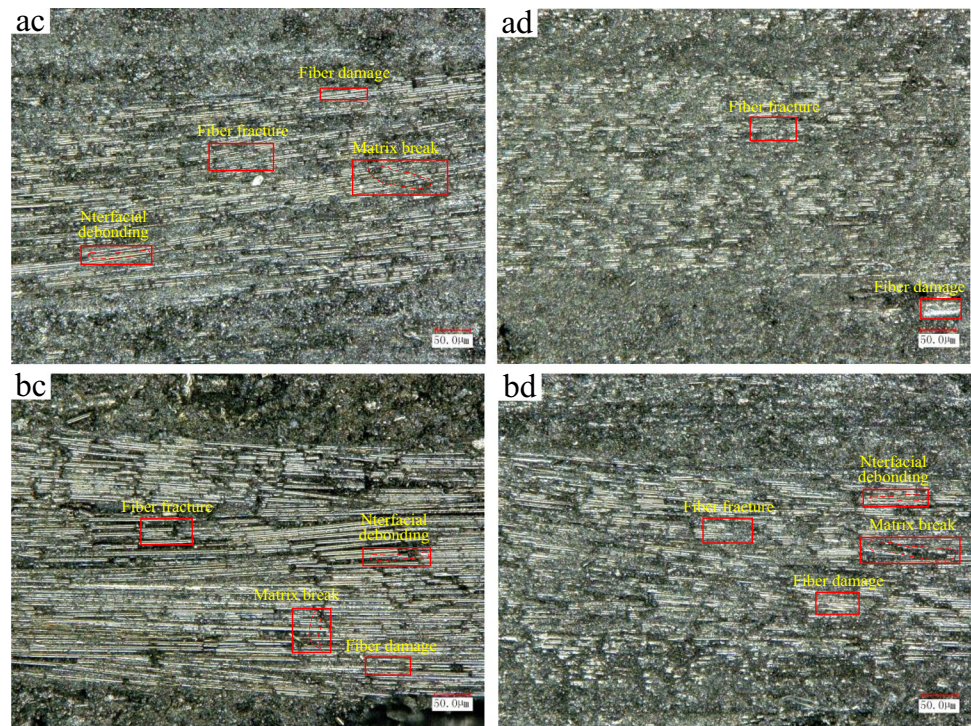
multiple-truncated short fibers by the impact of ultrasonic vibration, carbon fiber is eliminated in the form of short fiber and the breaking and peeling of the material during CG are decreased. The maximum heights of CG and L-TUVAG increase from 15.99 to 19.80 μm and 10.86 to 14.94 μm when the grinding depth is between 3 and 12 μm .

This surface topography of the CG and L-TUVAG is seen in Figs. 8 and 11, respectively, at 50 and 200 mm/min feed rates. The method of material removal did not change. The percentage of shorter fractures is maximum and the surface topography is flat when the feed speed is 50 mm/min. When the feed speed is 200 mm/min, longer cracks are more likely to occur, which denotes poor treated surface quality. Therefore, to obtain better surface quality, the propagation of long cracks must be prevented and it is best to employ a slower feed speed. L-TUVAG results in reduced cracks along with surface quality, as seen in Fig. 8d. Under the condition that the grinding conditions are guaranteed, L-TUVAG can pick a higher feed rate, which can improve the processing efficiency of materials. The maximum height of 3D surface topography in CG and L-TUVAG increases from 16.39 to 19.57 μm and 12.79 to 15.89 μm , respectively, when the feed speed is 50–200 mm/min.

9 3D Surface roughness

The quantitative relationship between surface roughness parameters and grinding wheel speed is shown in Fig. 12a. S_z , S_q , and S_a values of L-TUVAG are lower than CG.

Fig. 8 2D surface topography; $V_c = 3000$ rpm, $a_p = 6$ μm ; (a) $V_w = 50$ mm/min; (b) $V_w = 200$ mm/min; (c) CG; (d) L-TUVAG



Continuous separation-contact grinding occurs during machining because of high-frequency ultrasonic vibration. As a result, the continuous friction and impact between the abrasive particles and workpieces are reduced simultaneously, and the surface is smoother. The S_z , S_q , and S_a of CG and L-TUVAG clearly decline as the grinding wheel speed rises. S_z decreases rapidly as the grinding wheel speed rises from 2000 to 5000 rpm. The high peaks and troughs gradually approach the reference surface. The whole amount of diamond grains used in the grinding procedure increases along with the grinding speed. However, individual abrasives' lengths for grinding are cut down, and the normal force is reduced. A small normal force will only produce small cracks. The direction of the crack shifts when it approaches the intersection of fiber and matrix. The crack's energy is diminished, and as a result, the surface quality improved as well.

Figure 12b illustrates the changing trend of surface roughness parameters as the grinding depth increases from 3 to 12 μm . The surface roughness obviously increases as the grinding depth increases. These parameters might suggest that the machined surface gets progressively rougher and that the surface roughness degrades. It demonstrates that a key element in determining surface roughness is the grinding depth. The main removal methods for brittle ceramic materials are crack forming and propagation. The fibers merely direct the direction of the crack. Increased F_n and maximum undeformed chip thickness caused by increased grinding depth will hasten the spread and expansion of

cracks. According to Fig. 12b, L-TUVAG produces surfaces with roughness parameters that are considerably smaller than those produced by traditional grinding. Carbon fiber is truncated into multiple-segment short fibers during the L-TUVAG process, which improves surface quality and cuts down on crack propagation length.

As shown in Fig. 12c, S_z , S_q , and S_a of both CG and L-TUVAG are rising with feed speed, but the increasing trend is not very obvious. The Roughness parameter value does not significantly increase when the feed speed rises from 50 to 100 mm/min. However, as feed speed increases from 150 to 200 mm/min, S_z clearly increases, showing a decline in the quality of the machined surface. Although the lower feed speed in this study can improve the surface quality, the processing efficiency is low. The ultrasonic-assisted grinding can be used in actual production and processing to improve feed speed under the same grinding parameters.

10 Mechanism analysis of L-TUVAG

SiC matrix is a hard and brittle material that carbon fiber is not. As a result, the two removal methods are different and out of sync in the process of material removal via grinding. Brittle materials can be removed thanks to the creation and spread of cracks. The SiC matrix's plasticity, however, has been markedly improved by the carbon fiber reinforcement. Therefore, the removal mode of C_f /SiC materials has changed dramatically.

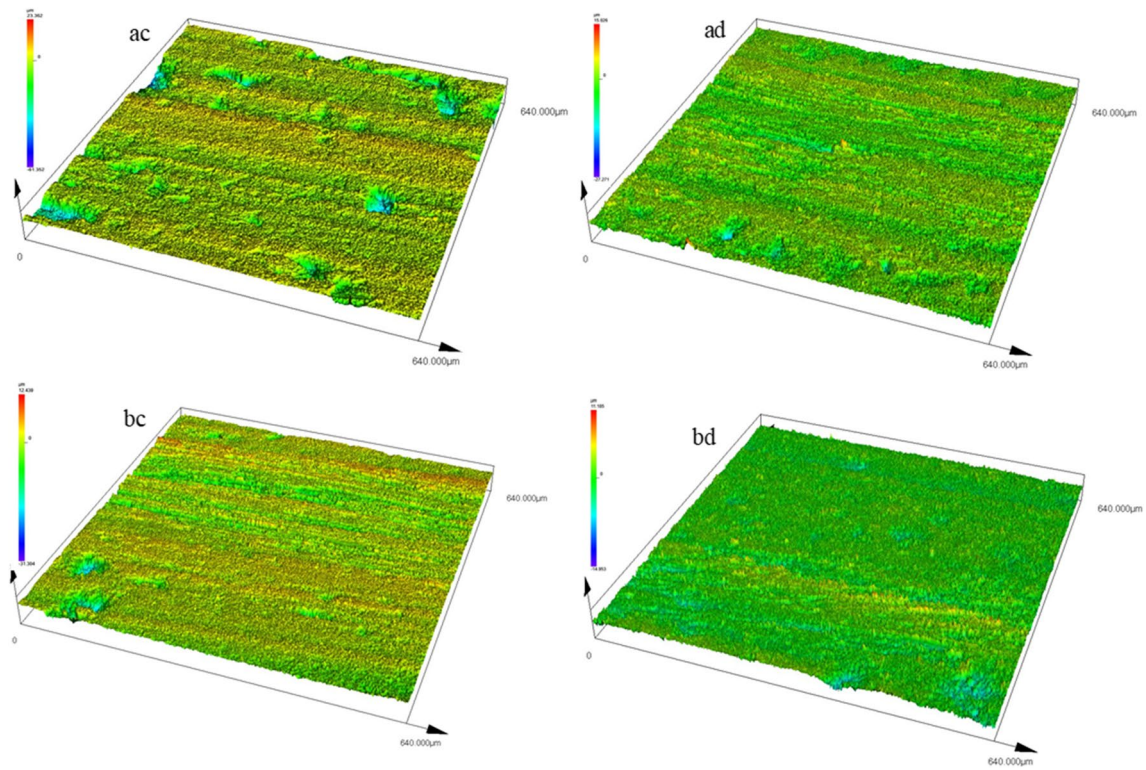


Fig. 9 3D surface topography; $a_p = 6 \mu\text{m}$, $V_w = 100 \text{ mm/min}$; (a) $V_c = 2000 \text{ rpm}$; (b) $V_c = 5000 \text{ rpm}$; (c) CG; (d) L-TUVAG

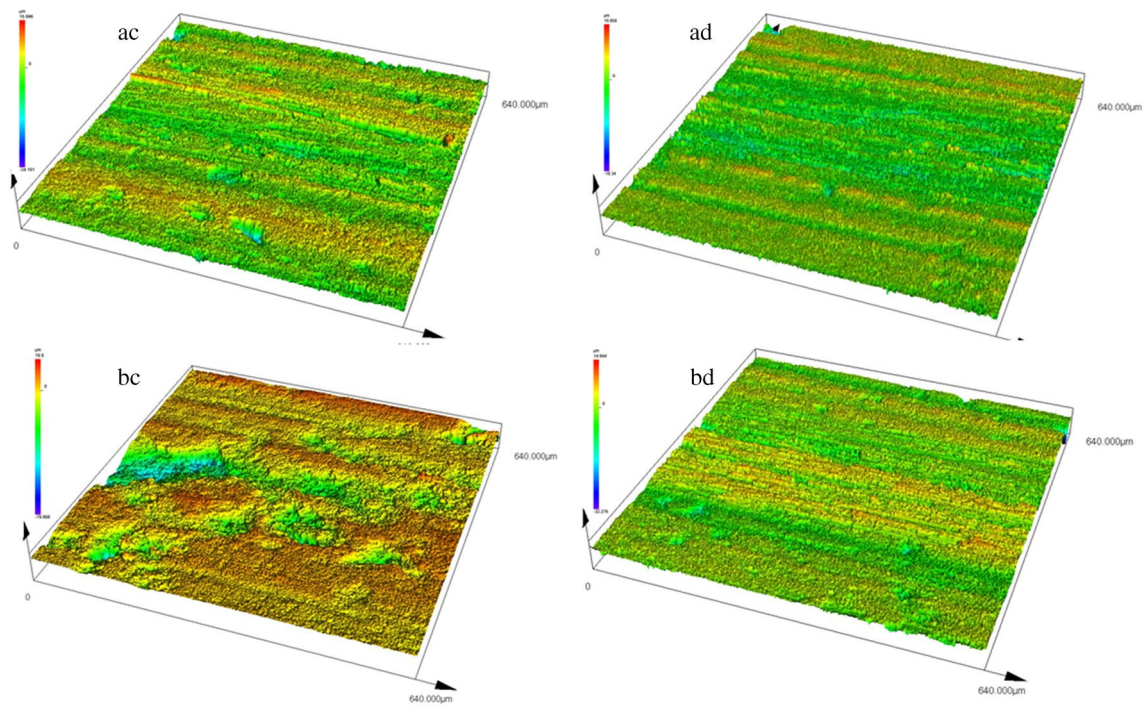


Fig. 10 3D surface topography; $V_c = 3000 \text{ rpm}$, $V_w = 100 \text{ mm/min}$; (a) $a_p = 3 \mu\text{m}$; (b) $a_p = 12 \mu\text{m}$; (c) CG; (d) L-TUVAG

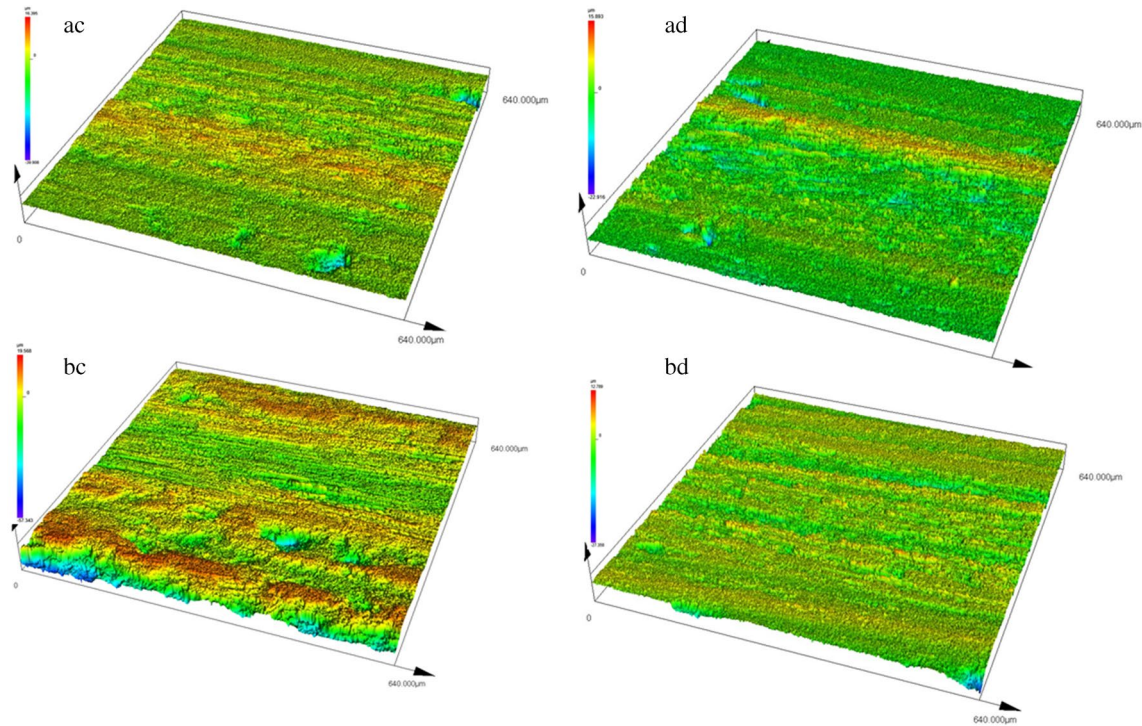
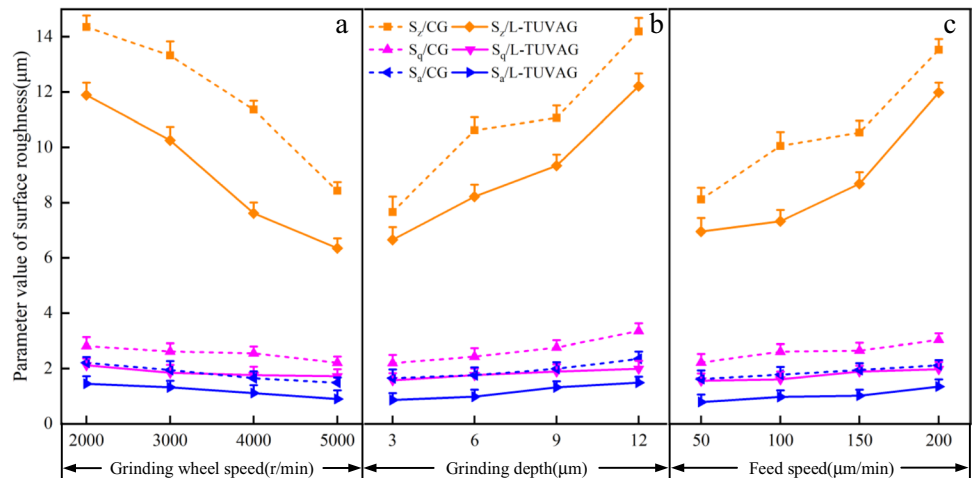


Fig. 11 3D surface topography; $V_c = 3000$ rpm, $a_p = 6 \mu\text{m}$; (a) $V_w = 50$ mm/min; (b) $V_w = 200$ mm/min; (c) CG; (d) L-TUVAG

The materials were processed in the orthogonal plane, and the 0° and 90° fibers and the SiC matrix were simultaneously removed by grinding wheels. First, the SiC matrix is harmed by the shear and extrusion of the grinding wheel. The process will result in numerous cracks. The fiber's limitations, however, increase its toughness and limit the spread of cracks. The 0° fiber will be sheared and extruded when the abrasive comes into contact with it. Due to the weak interfacial adhesion, as seen in Figs. 7c and 8c, the cracks spread along the fiber direction and are prone to longer cracks. As a result, fiber damage and interfacial debonding are frequently

seen on processed surfaces. The SiC matrix undergoes high-frequency impact as well as abrasive shear and extrusion during L-TUVAG, as seen in Figs. 7d and 8d, and the matrix is removed with smaller particles, leading to smaller and fewer cracks. Under ultrasonic high-frequency impact, the 0° fiber is truncated into a multiple-segment short fiber, which prevents the crack from spreading in the fiber direction. Interfacial debonding and fiber damage are not obvious processes. The 90° fiber is sliced and extruded by the abrasive particles as they come into contact with it, which causes fiber deformation. When shear force is greater than shear strength, the

Fig. 12 Surface roughness 3D parameters as a function of grinding wheel speed; (a) $a_p = 6 \mu\text{m}$, $V_w = 100$ mm/min; (b) $V_c = 3000$ rpm, $V_w = 100$ mm/min; (c) $V_c = 3000$ rpm, $a_p = 6 \mu\text{m}$



fiber breaks, the crack's extension abruptly comes to a halt or changes course, and the fracture continues to expand due to the energy still present in it. In L-TUVAG, the 90° fiber is first severed by high-frequency impact, and removed by abrasive, which lessens fracture expansion and causes smaller cracks to form. Additionally, the surface topography is good as seen in Figs. 9d and 10d. The materials under study also contain a significant number of needled structures, as seen in Fig. 3, which strengthen the bonding between the fiber bundles and significantly slow down fracture spread.

The fundamental removal forms of the materials are matrix breaks, interfacial debonding, fiber damage, and fractures, as seen in Figs. 6, 7, and 8. The quantity of abrasive particles used in processing reduces as grinding wheel speed increases. Each abrasive's cutting thickness decreases while maintaining the same grinding depth, resulting in a shallower and shallower grinding groove and steadily improving surface quality. Figures 9, 10, and 11 show the flaws become more visible as feed speed and grinding depth raise over time because matrix and fiber are subjected to higher shear and extrusion pressures (Fig. 12).

11 Conclusion

In this paper, L-TUVAG and CG experiments were carried out on 2.5D needled C_f/SiC materials. The effect of different grinding parameters on the grinding force was investigated. The material removal mechanism was analyzed, and the surface topography of the ground material was observed after grinding. Examine the effects of the grinding factors on the three-dimensional surface roughness characteristics of the materials. These characteristics are summarized in the following: 1. Under the same grinding parameters, the maximum undeformed cutting thickness of L-TUVAG is less than CG. L-TUVAG has a significantly lower grinding force than CG. The force needed to grind with L-TUVAG can be greatly reduced while simultaneously making the processing surface's quality better. The grinding force can be decreased by 26.85–45.23% in comparison to the CG process, and the surface roughness value is also considerably reduced.

2. The brittle crack is the main reason why materials are removed. The primary removal methods are matrix breaks, interfacial debonding, fiber damage and fractures. The two main removal types can be determined by examining the topography of the machined surface: matrix crack and fiber fracture. CG removes carbon fibers from the matrix and leaves grooves behind; L-TUVAG splits carbon fibers into numerous short fibers through ultrasonic high-frequency impact, which is followed by removal as short fibers. The carbon fiber's propensity to split and peel are reduced.

3. CG and L-TUVAG surface quality have been shown through grinding experiments to improve with increasing grinding wheel speed while decreasing with increasing the

feed speed and grinding depth. More specifically, as the grinding wheel speed rises, the values of S_a , S_z , and S_q decrease consistently. Under the same circumstances, the abrasive trajectory of L-TUVAG is longer than CG. L-TUVAG can increase abrasive grinding time, reduce the residual height of materials on the workpiece surface, improve the surface quality of the workpiece, and reduce the surface roughness.

Author contribution All authors contributed to the study conception and design. Xiaobo Wang: project administration, formal analysis, writing—review and editing. Mingqiang Wu: methodology, investigation, formal analysis, writing—review and editing. Chaosheng Song: data curation, investigation. Bo Zhao: writing—review and editing.

Funding Financial support for the research, authorship, and/or publication is provided by the National Natural Science Foundation of China (No.52005164).

Declarations

Conflict of interest The authors declare no competing interests.

References

- Zhang H, Yang Y, Hu K, Liu B, Liu M, Huang ZR (2020) Stereolithography-based additive manufacturing of lightweight and high-strength C_f/SiC ceramics. *Addit Manuf* 34:101199
- Chen TF, Cheng S, Jin LZ, Xu TT, Zeng T (2021) Fabrication process and mechanical properties of C/SiC corrugated core sandwich panel. *Ceram Int* 47:3634–3642
- He ZB, Chen B, Zhang Y, Liu YS, Zhang LT (2019) Mechanical behavior of C/SiC T-section under pulling load. *J Mater Sci Technol* 35:2950–2956
- Wang YL, Wang WL, Huang J, Ye ZH, Yang J, Chen SH (2021) Joining of C_f/SiC composite and 304 stainless steel assisted by surface honeycomb modification. *J Eur Ceram Soc* 41:6824–6833
- Rösiger A, Goller R, Langhof N, Krenkel W (2021) Influence of in-plane and out-of-plane machining on the surface topography, the removal mechanism and the flexural strength of 2D C/C-SiC composites. *J Eur Ceram Soc* 41:3108–3119
- Zhou K, Xu JY, Xiao GJ, Huang Y (2022) A novel low-damage and low-abrasive wear processing method of C_f/SiC ceramic matrix composites: laser-induced ablation-assisted grinding. *J Mater Process Technol* 302:117503
- Chen J, An QL, Chen M (2020) Transformation of fracture mechanism and damage behavior of ceramic-matrix composites during nano-scratching. *Compos A Appl Sci Manuf* 130:105756
- Xie ZW, Liu ZQ, Wang B, Xin MZ, Song QH, Jiang LP (2021) Longitudinal amplitude effect on material removal mechanism of ultrasonic vibration-assisted milling 2.5 DC/SiC composites. *Ceram Int* 47:32144–32152
- Yang YY, Qu SS, Gong YD (2021) Investigating the grinding performance of unidirectional and 2.5 D C/SiCs. *Ceram Int* 47:5123–5132
- Zhou K, Xiao GJ, Xu JY, Huang Y (2021) Material removal behavior of C_f/SiC ceramic matrix composites as a function of abrasive wear during diamond abrasive belt grinding. *Wear* 486:204101
- Lei XF, Xiang DH, Peng PC, Liu GF, Li B, Zhao B, Gao GF (2022) Establishment of dynamic grinding force model for

- ultrasonic-assisted single abrasive high-speed grinding. *J Mater Process Technol* 300:117420
12. Agarwal S, Rao PV (2010) Grinding characteristics, material removal and damage formation mechanisms in high removal rate grinding of silicon carbide. *Int J Mach Tools Manuf* 50:1077–1087
 13. Xiong YF, Wang WH, Jiang RS, Huang B, Liu C (2022) Feasibility and tool performance of ultrasonic vibration-assisted milling-grinding SiCf/SiC ceramic matrix composite. *J Mater Res Technol* 19:3018–3033
 14. Fan SW, Zhang LT, Cheng LF, Yang SG (2011) Microstructure and frictional properties of C/SiC brake materials with sandwich structure. *Ceram Int* 37:2829–2835
 15. Zhang LF, Ren CZ, Ji CH, Wang ZQ, Chen G (2016) Effect of fiber orientations on surface grinding process of unidirectional C/SiC composites. *Appl Surf Sci* 366:424–431
 16. Cao XY, Lin B, Wang Y, Wang SL (2014) Influence of diamond wheel grinding process on surface micro-topography and properties of SiO₂/SiO₂ composite. *Appl Surf Sci* 292:181–189
 17. An QL, Chen J, Ming WW, Chen M (2021) Machining of SiC ceramic matrix composites: a review. *Chin J Aeronaut* 34(4):540–567
 18. Xiong YF, Liu C, Wang WH, Jiang RS, Huang B, Wang DH, Zhang SG (2023) Assessment of machined surface for SiC_f/SiC ceramic matrix composite during ultrasonic vibration-assisted milling-grinding. *Ceram Int* 49:5345–5356
 19. Kumar J (2013) Ultrasonic machining—a comprehensive review. *Mach Sci Technol* 17:325–379
 20. Ding K, Fu Y, Su HH, Chen Y, Yu XZ, Ding GZ (2014) Experimental studies on drilling tool load and machining quality of C/SiC composites in rotary ultrasonic machining. *J Mater Process Technol* 214:2900–2907
 21. Wang H, Ning FD, Li YC, Hu YB, Cong WL (2019) Scratching-induced surface characteristics and material removal mechanisms in rotary ultrasonic surface machining of CFRP. *Ultrasonics* 97:19–28
 22. Wang DP, Lu SX, Xu D, Zhang YL (2020) Research on material removal mechanism of C/SiC composites in ultrasound vibration-assisted grinding. *Materials* 13:1918
 23. Cao JG, Wu YG, Lu D, Fujimoto M, Nomura M (2014) Fundamental machining characteristics of ultrasonic assisted internal grinding of SiC ceramics. *Mater Manuf Process* 29:557–563
 24. Wang JJ, Zhang JF, Feng PF (2017) Effects of tool vibration on fiber fracture in rotary ultrasonic machining of C/SiC ceramic matrix composites. *Compos B Eng* 129:233–242
 25. Choudhary A, Chakladar ND, Paul S (2021) Identification and estimation of defects in high-speed ground C/SiC ceramic matrix composites. *Compos Struct* 261:113274
 26. Azarhoushang B, Tawakoli T (2011) Development of a novel ultrasonic unit for grinding of ceramic matrix composites. *Int J Adv Manuf Technol* 57:945–955
 27. Bertsche E, Ehmann K, Malukhin K (2013) Ultrasonic slot machining of a silicon carbide matrix composite. *Int J Adv Manuf Technol* 66:1119–1134
 28. Yuan SM, Fan HT, Amin M, Zhang C, Guo M (2016) A cutting force prediction dynamic model for side milling of ceramic matrix composites C/SiC based on rotary ultrasonic machining. *Int J Adv Manuf Technol* 86:37–48
 29. Liu Q, Huang GQ, Fang CF, Cui CC, Xu XP (2017) Experimental investigations on grinding characteristics and removal mechanisms of 2D-C_f/C-SiC composites based on reinforced fiber orientations. *Ceram Int* 43:15266–15274
 30. Qu SS, Gong YD, Yang YY, Wen XL, Yin GQ (2019) Grinding characteristics and removal mechanisms of unidirectional carbon fiber reinforced silicon carbide ceramic matrix composites. *Ceram Int* 45:3059–3071
 31. Malkin S, Guo C (2008) Grinding technology: theory and application of machining with abrasives[M]. Industrial Press Inc

Publisher's note Springer Nature remains neutral with regard to jurisdictional claims in published maps and institutional affiliations.

Springer Nature or its licensor (e.g. a society or other partner) holds exclusive rights to this article under a publishing agreement with the author(s) or other rightsholder(s); author self-archiving of the accepted manuscript version of this article is solely governed by the terms of such publishing agreement and applicable law.